Photothermal-responsive nanosized hybrid polymersome as versatile therapeutics codelivery nanovehicle for effective tumor suppression

Hongbo Zhang[a,b,c,d,1], Wenguo Cui[b,e,1], Xiangmeng Qu[a,b,1,2], Huayin Wu[b,1], Liangliang Qu[a,b], Xu Zhang[b,3], Ermei Mäkilä[f], Jarno Salonen[f], Yueqi Zhu[g,4], Zhou Yang[a], Dong Chen[b], Hélder A. Santos[h], Mingtan Hai[a,b,4], and David A. Weitz[b,i,4]

[a]Beijing Key Laboratory of Function Materials for Molecule and Structure Construction, School of Materials Science and Engineering, University of Science and Technology Beijing, Beijing 100083, People's Republic of China; [b]Harvard John A. Paulson School of Engineering and Applied Sciences, Harvard University, Cambridge, MA 02138; [c]Department of Pharmaceutical Sciences Laboratory, Åbo Akademi University, FI-20520 Turku, Finland; [d]Turku Center for Biotechnology, University of Turku and Åbo Akademi University, FI-20520 Turku, Finland; [e]Shanghai Institute of Traumatology and Orthopaedics, Ruijin Hospital, Shanghai Jiao Tong University School of Medicine, Shanghai 200025, People's Republic of China; [f]Laboratory of Industrial Physics, Department of Physics, University of Turku, FI-20014 Turku, Finland; [g]Department of Interventional Radiology, Shanghai Jiao Tong University Affiliated Sixth People's Hospital, Shanghai 200233, People's Republic of China; [h]Division of Pharmaceutical Chemistry and Technology, Helsinki Institute of Life Science, University of Helsinki, FI-00014 Helsinki, Finland; and [i]Department of Physics, Harvard University, Cambridge, MA 02138

Edited by Tobin J. Marks, Northwestern University, Evanston, IL, and approved March 6, 2019 (received for review October 10, 2018)

Effective cancer therapies often demand delivery of combinations of drugs to inhibit multidrug resistance through synergism, and the development of multifunctional nanovehicles with enhanced drug loading and delivery efficiency for combination therapy is currently a major challenge in nanotechnology. However, such combinations are more challenging to administer than single drugs and can require multipronged approaches to delivery. In addition to being stable and biodegradable, vehicles for such therapies must be compatible with both hydrophobic and hydrophilic drugs, and release drugs at sustained therapeutic levels. Here, we report synthesis of porous silicon nanoparticles conjugated with gold nanorods [composite nanoparticles (cNPs)] and encapsulate them within a hybrid polymersome using double-emulsion templates on a microfluidic chip to create a versatile nanovehicle. This nanovehicle has high loading capacities for both hydrophobic and hydrophilic drugs, and improves drug delivery efficiency by accumulating at the tumor after i.v. injection in mice. Importantly, a triple-drug combination suppresses breast tumors by 94% and 87% at total dosages of 5 and 2.5 mg/kg, respectively, through synergy. Moreover, the cNPs retain their photothermal properties, which can be used to significantly inhibit multidrug resistance upon near-infrared laser irradiation. Overall, this work shows that our nanovehicle has great potential as a drug codelivery nanoplatform for effective combination therapy that is adaptable to other cancer types and to molecular targets associated with disease progression.

nanomaterials | drug delivery | cancer therapy | microfluidics

Recent advances in cancer therapy development often demand the simultaneous delivery of multiple drugs that work in a synergistic manner (1–4). These drugs can vary in their chemical properties, further adding complexity to their encapsulation and delivery. Delivery systems can suffer from low loading efficiencies, particularly when combinations of both hydrophobic and hydrophilic drugs are required. Hydrophobic anticancer drugs face additional significant barriers to their use as they have low bioavailability and are rapidly eliminated from the body. In vivo, delivery of drug combinations (5, 6) requires specific, biodegradable vehicles to protect the therapeutics from the physiological environment and to guide and control their release (7–14). Additionally, stimuli-responsive treatments are increasingly widely used to complement drug-based therapy (15–19). For example, photothermal therapy promotes cell death using heat that is locally activated by near-infrared (NIR) radiation (20). However, it is challenging to integrate high drug-loading efficiency, the ability to coload multiple therapeutics, and stimuli responsiveness into a single carrier system. Carriers that move toward realizing these multipronged approaches to cancer therapy will push the frontiers of drug delivery and enable the development of new, more effective treatments.

In this work, we synthesize porous silicon nanoparticles (PSi NPs) conjugated with gold nanorods (AuNRs) [composite nanoparticles (cNPs)] to achieve high drug-loading capacity and photothermal responsiveness. Subsequently, a robust microfluidic technique is used to create hybrid polymersomes using water-in-oil-in-water (w/o/w) emulsion templates for encapsulation of cNPs. The hybrid polymersomes are composed of a combination of poly(ethylene glycol)-b-poly(lactic acid) diblock copolymers and

Significance

The use of increasingly sophisticated drugs to treat diseases like cancer often requires increasingly sophisticated delivery technologies, where multiple drugs often must be delivered simultaneously and in precise amounts; moreover, many drugs are hydrophobic and cannot be easily delivered. We report a simple and robust process to fabricate nanometer-sized polymersomes that can simultaneously deliver multiple therapeutics, both hydrophobic and hydrophilic, and have significantly improved drug-loading efficiencies over existing methods. We use these polymersomes to deliver a combination of hydrophobic anticancer drugs in a mouse model and see remarkable effectiveness against breast tumors. This work enables the use of previously undeliverable compounds in cancer therapy and forms a foundation for further development in a broad range of biomedical applications.

Author contributions: M.H. and D.A.W. designed research; H.Z., W.C., X.Q., L.Q., X.Z., E.M., J.S., Y.Z., and D.C. performed research; H.Z., W.C., X.Q., L.Q., X.Z., E.M., J.S., Y.Z., Z.Y., D.C., H.A.S., and M.H. analyzed data; and H.Z., H.W., H.A.S., M.H., and D.A.W. wrote the paper.

The authors declare no conflict of interest.

This article is a PNAS Direct Submission.

[1]H.Z., W.C., X.Q., and H.W. contributed equally to this work.

[2]Present address: School of Biomedical Engineering, Sun Yat-Sen University, Guangzhou 510006, People's Republic of China.

[3]Present address: Department of Chemistry, Cape Breton University, Sydney, NS B1P 6L2, Canada.

[4]To whom correspondence may be addressed. Email: zhuyueqi@hotmail.com, mingtanhai@mater.ustb.edu.cn, or weitz@seas.harvard.edu.

This article contains supporting information online at www.pnas.org/lookup/suppl/doi:10.1073/pnas.1817251116/-/DCSupplemental.

phospholipids to achieve high biocompatibility and low permeability. A final extrusion step is used to generate stable nanometer-sized hybrid polymersomes. We show that the nano-polymersomes act as nanovehicles that have high loading capacity for both hydrophobic and hydrophilic drugs and have photothermal responsiveness. A combination of three hydrophobic drugs that was previously only deliverable orally is loaded into the nanovehicles, delivered intravascularly, and shown to very effectively suppress breast cancer tumors at low dosages in a mouse model (Scheme 1). Moreover, the constructed nanovehicle is versatile; by also loading magnetic nanoparticles, DNA, or antibodies, they can be adapted for more specialized applications along with NIR photothermal combination therapy.

To create these cNPs, we first use seed-mediated growth to fabricate AuNRs (21, 22) about 50 nm in length (*SI Appendix*, Fig. S1*A*) with a surface plasmon resonance peak around 975 nm (*SI Appendix*, Fig. S1). In parallel, we use electrochemical etching methods to fabricate PSi NPs with a carboxyl surface group (23). The PSi NPs are 150 nm in diameter, as measured by dynamic light scattering (DLS). The PSi NPs are then conjugated with AuNRs to create cNPs through a two-step chemical reaction. The carboxyl surface groups of the PSi NPs are activated by *N*-(3-dimethylaminopropyl)-*N*′-ethylcarbodiimide hydrochloride (EDC) for half an hour under magnetic stirring at 25 °C and reacted with the amine group of cysteamine ($HNCHCH_2SH$) for 24 h at 25 °C. Then, the HS group of PSi-$CONCHCH_2$-HS is easily connected with the AuNRs to produce the final cNPs structure. A scanning electron microscopy (SEM) image of the synthesized cNPs is shown in *SI Appendix*, Fig. S1*B*. A high concentration of cNPs is dried on the wafer for imaging, which results in the aggregation seen in the figure. The cNPs have a diameter of 159 nm when measured by DLS. The plasmon resonance peak around 930 nm shows the photothermal property of cNPs (*SI Appendix*, Fig. S1). An X-ray photoelectron spectroscopy spectrum confirms the successful reaction of the cNPs (*SI Appendix*, Fig. S2).

After production, the cNPs are loaded with drugs through a simple adsorption process. First, the cNPs are dispersed in pure ethanol by sonication. Afterward, hydrophobic anticancer drugs are added to the cNPs suspension under magnetic stirring for 6 h during which they adsorb to the nanoparticles. The drug-loaded cNPs are separated from the ethanol solution by centrifugation at 14,100 × *g*. Importantly, cNPs carrying either hydrophilic or hydrophobic drugs can still be well dispersed in water, so they can be easily encapsulated into the hybrid polymersome water

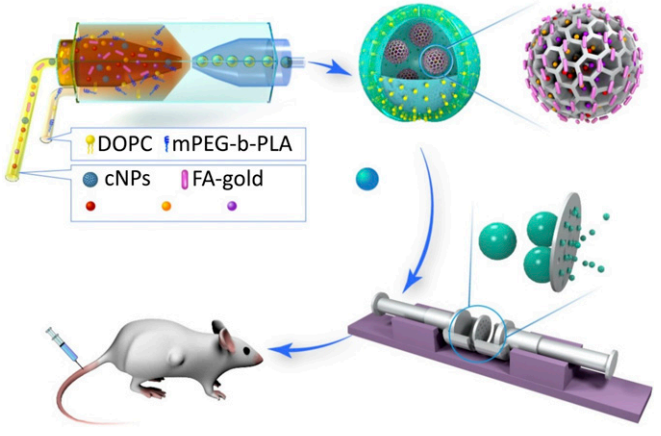

Scheme 1. The fabrication of photothermal-responsive nanosized hybrid polymersome as versatile therapeutics codelivery nanovehicle for i.v. injection cancer treatment.

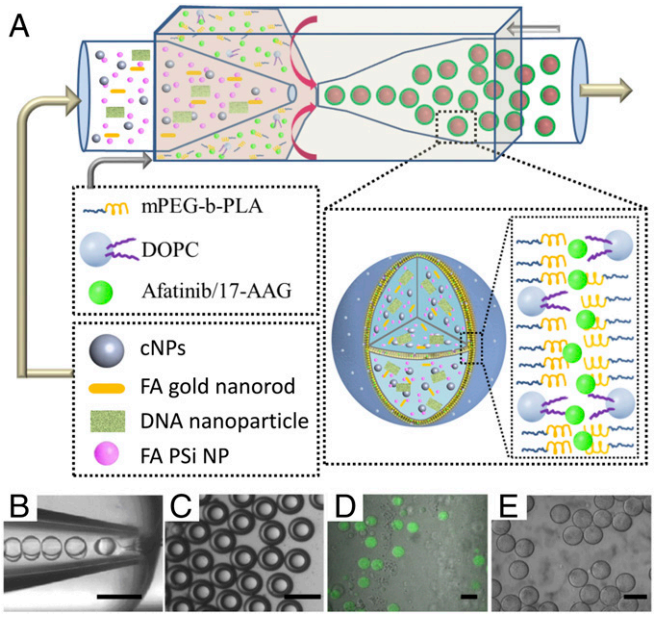

Fig. 1. Generation of cNPs-functionalized hybrid polymersomes vehicle. (*A*) Scheme of the generation of monodisperse double-emulsion templates for encapsulation of cNPs, folate-conjugated AuNRs, and folate-conjugated PSi NPs. (*B*) Optical microscope image showing the w/o/w emulsion droplets formation using microfluidics. (Scale bars: 100 μm.) (*C*) The collected hybrid polymersomes w/o/w double-emulsion droplets. (Scale bars: *B* and *C*, 100 μm.) (*D*) Confocal images of hybrid polymersomes encapsulating DOX. (Scale bar: 50 μm.) (*E*) Confocal image of the hybrid polymersomes alone. (Scale bar: 50 μm.)

core, which greatly improves the drug-loading capacity of the nanovehicle.

We encapsulate cNPs into the core–shell hybrid polymersome using a w/o/w emulsion template with three separate phases (23–26) that is made using microfluidic techniques combining coflow and flow focusing geometries (23–26), as shown in Fig. 1*A* and Movie S1. The inner water phase contains 400 μg/mL cNPs in a 4 wt% polyvinyl alcohol (PVA) aqueous solution and the outer water phase is a 10 wt% PVA aqueous solution with an osmolarity of 100 mOsm/L. The middle oil phase contains 10 mg/mL of an amphiphilic diblock copolymer, mPEG(5000)-b-PLA(10000), and 2 mg/mL of a phospholipid, 1,2-dioleoyl-*sn*-glycero-3-phosphocholine (DOPC), dissolved in a mixture of chloroform and hexane. In the microfluidic device, the hydrodynamically focused inner and middle phase fluid streams break up at the orifice of the collection tube to form a monodisperse w/o/w emulsion, as shown in Fig. 1*B*. The collected w/o/w emulsion droplets are uniform in size and structure (Fig. 1*C*), making them ideal templates for the formation of drug delivery vehicles (Fig. 1 *D* and *E*). By changing the flow rates of each fluid phase and the diameters of each capillary in the device, the overall size of the double emulsion droplets can be adjusted between 50 to 150 μm (24). Furthermore, when the inner flow rate is high enough to match that of the middle phase, the resultant droplets have ultrathin shells, less than 10% oil phase by volume (Fig. 1*B*). Ultrathin shell droplets are significantly more stable because lubrication forces greatly slow the migration of the inner drop to the outer wall and prevent coalescence of the inner drop with the continuous fluid. A dewetting process, where the double emulsions transition from complete wetting to partial wetting at the middle oil phase, forms the hybrid bilayer shells. In our system, chloroform, whose solubility is around 8 g/L in water, evaporates at a much faster rate than hexane, whose solubility is around 13 mg/L. The solvent mixture becomes increasingly hexane-rich and eventually turns into a poor solvent for

the diblock copolymer and phospholipid molecules, which leads to attraction between the two compounds and precipitation. Here, the thin shell also minimizes the amount of residual solvent within the vehicle membrane, and thus overcomes the limited biocompatibility of vesicles fabricated by typical microfluidic approaches.

The relationship between chloroform volume fraction and adhesion strength implies that reducing the chloroform volume fraction should promote the formation of polymersomes. However, we only observe polymersome formation and dewetting when the volume fraction of the chloroform is between 36% and 42%. We measure the contact angles at the three-phase contact line and find that volume fractions outside this range have small contact angles, which lead to wetting at the interfaces and thus double-emulsion droplets cannot be generated (Fig. 2*A*). This result is consistent with previous reports of the formation of mPEG(5000)-b-PLA (5000) polymersomes upon dewetting (25, 26). The vehicles reported here are formed using a chloroform-to-hexane volume ratio of 38:62.

Although the introduction of phospholipids in polymersomes enhances biocompatibility, it also decreases the membrane strength and stability. Thus, the ratio of copolymer to phospholipid is a crucial parameter. To find a composition that balances these effects, we begin with copolymer and add phospholipid to the system in weight ratios of 10:0, 10:1; 10:2, and 10:3. To compare the stability of pure polymersomes and hybrid polymersomes with different lipid ratios, we incubate the various polymersomes in the same 100 mOsm/L aqueous solution and use microscopy to quantify the remaining number every 7 d over the course of 1 mo. We find that the higher the lipid content, the fewer polymersomes remain after 1 mo (*SI Appendix*, Table S1). Thus, we conclude that the stability of the hybrid polymersomes is decreased with increased lipid content. In parallel, viability studies on M28 cells incubated with polymersomes for 24 h at 37 °C verify that biocompatibility is improved at ratios of at least 10:2, as shown in Fig. 2*B*. Since further increases in the ratio only minimally change biocompatibility, we select 10:2 as the optimum ratio of copolymer to phospholipid for the hybrid polymersomes.

The final step of fabrication involves extrusion of the hybrid polymersomes through a 0.2-μm membrane filter to fabricate nanometer-sized hybrid polymersomes, as confirmed by cryo-transmission electron microscopy (cryo-TEM) imaging (Fig. 2*C*). The hydrodynamic diameter of empty nanovehicles is 156 ± 32 nm with a polydispersity index of 0.16 when measured by DLS at 25 °C.

We evaluate the cytocompatibility of the nanovehicles using HeLa Nulight red cells and M28 cells. After incubation with nanovehicles for 24 h at 37 °C, the viability of both HeLa and M28 cells is above 90%, as shown in *SI Appendix*, Figs. S3 and S4. By comparison, cells incubated without any nanovehicles exhibited viabilities of at least 92%. This result indicates that the nanovehicle itself is cytocompatible and any effect on viability is due to the cargo.

To test the drug delivery capability of the nanovehicles, we select a combination of three hydrophobic anticancer drugs: docetaxel (D), rapamycin (R), and afatinib (A). Docetaxel is one of the most effective chemodrugs for breast cancer treatment and a standard second-line therapy for lung cancer. Rapamycin has immunosuppressant function, and, at appropriate doses, it has been shown to promote tumor suppression in clinical trials (27–31). Afatinib is a molecular-targeting drug that inhibits both HER2 and EGFR, and has been used against both breast cancer and lung cancer (32, 33). We expect such a drug combination to be very effective at suppressing HER2-positive breast tumors and EGFR-positive lung tumor, but the drug hydrophobicity has presented a significant challenge to their delivery, and this combination has not previously been used.

The encapsulation efficiency of cNPs in nanovehicles is above 92% when generated using microfluidic double-emulsion templates. Using the same extrusion method and a 0.4-μm membrane filter, nanovehicles containing cNPs loaded with three drugs have a hydrodynamic diameter of 286 ± 79 nm (Fig. 2*D*). The peak in the DLS result is less than twice the diameter of a cNP, indicating that the majority of the nanovehicles should contain only one cNP, although some nanovehicles may be empty or contain multiple cNPs. While cryo-TEM characterization would ideally confirm this, we have found that these samples are unable to withstand the processing required to prepare samples for cryo-TEM imaging.

Additionally, the loading content of the different drugs is determined from the drug and vehicle weights. We find that when the encapsulated cNPs are loaded with docetaxel, rapamycin, afatinib, or any combination of these hydrophobic drugs, the maximum total degree of drug loading is about 20% by weight, regardless of the number of drugs. Because the drug-loading degree is mainly dependent on the overall amount of cNPs in the sample, the number that are encapsulated within any single nanovehicle should not affect the drug-loading capacity. Since the dose is calculated by using the drug-loading degree, the presence of empty nanovehicles will result in a slight increase of in the overall dose of nanovehicles. However, the empty nanovehicles are biocompatible and will not adversely affect the therapeutic effect, provided that the necessary amount of drug is delivered.

The dissolution rate of free DOX in phosphate buffer solution (PBS) (pH 7.4) is very fast; in contrast, no initial burst release is observed for any of the encapsulated compounds, and within 24 h, about 60–90% of the therapeutics are released in the buffer, as shown by the in vitro dynamic release profiles of the therapeutics in Fig. 3*A*. This controlled release is ideal in cancer

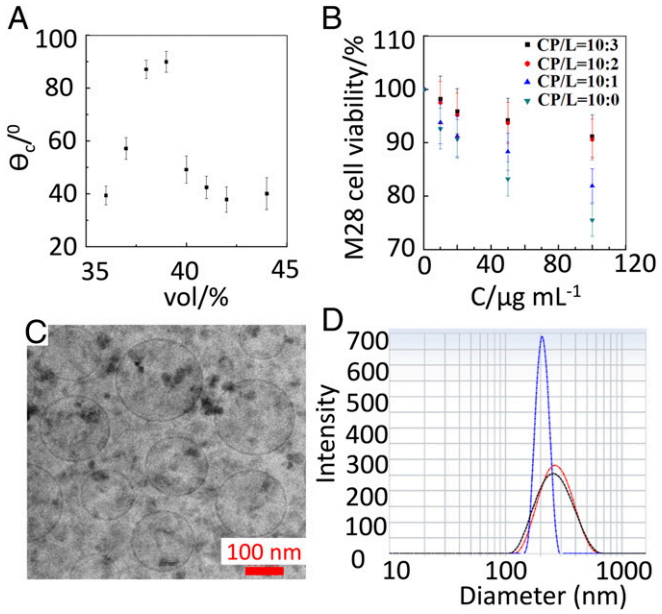

Fig. 2. The hybrid polymersomes vehicle formation, biocompatibility, and morphology study. (*A*) Plot of the contact angle (θ_C) of the solvent droplets of the polymersomes as a function of the fraction of the solvent chloroform. The volume fraction of chloroform in the solvent mixture was determined before the injection into the device. (*B*) The effect of ratio between copolymer (CP) and phospholipid (L) for the formation of the polymersomes on the cell viability after 24-h incubation with M28 at 37 °C. (*C*) The cryo-TEM image of the nanosized hybrid polymersomes nanovehicle after extrusion from 0.2-μm membrane. (Scale bar: 100 nm.) (*D*) The hydrodynamic diameter of the cNPs-functionalized hybrid nanovehicle after extrusion from 0.4-μm membrane measured by dynamic light scattering (DLS) at 298 K. Blue curve, One-drug–loaded nanovehicle; black curve, two-drug–loaded nanovehicle; red curve, three-drug–loaded nanovehicle.

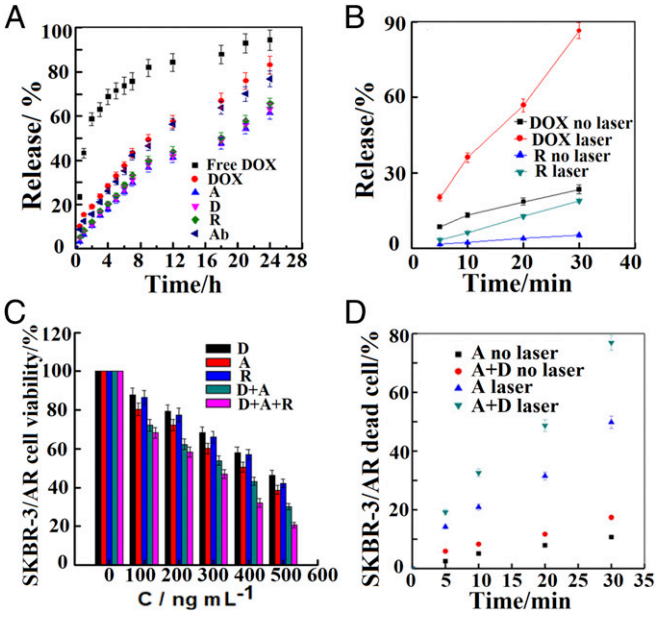

Fig. 3. In vitro release, photothermal effects and MDR inhibition study. (*A*) Therapeutics release from the hybrid polymersomes PBS suspension at 37 °C. Free DOX, DOX, afatinib (A), docetaxel (D), rapamycin (R), and antibody (Ab)-loaded hybrid polymersomes. (*B*) Photothermal effects induced by laser irradiation at 808-nm NIR laser wavelength of the cNPs on the release of DOX and rapamycin (R) at different time intervals. (*C*) The effect on afatinib-resistant SKBR-3/AR HER2-positive breast cancer cells proliferation of docetaxel (D), afatinib (A), rapamycin (R), D+A, and D+A+R-loaded hybrid polymersomes (C_D/C_A = 1:1, C_D/C_R = 1:1, $C_D/C_A/C_R$= 1:1:1 with 400 μg/mL cNPs set up as control) after 24-h incubation at 37 °C. (*D*) Cell viability of afatinib (A), afatinib-plus-docetaxel (D)-loaded functionalized nanovehicle under NIR laser irradiation at 808 nm at different time intervals or without laser irradiation on SKBR-3/AR cells after 2-h incubation using live/dead assay.

therapy to reduce the adverse side effects of the drugs (21, 22, 32, 33). In our nanovehicles, sustained release of therapeutics is achieved due to protection by the cNPs within the hybrid polymersome core.

In the nanovehicle core, 50-nm-long AuNRs are conjugated with the PSi NPs to provide photothermal functionality. The AuNRs and cNPs have a peak plasmonic resonance at 975 and 930 nm, making them particularly well-suited for biomedical applications since surrounding tissues absorb very little in this range. In addition, NIR laser irradiation of the AuNRs can trigger the release of hydrophilic chemodrugs such as doxorubicin hydrochloride (DOX). The release of DOX and rapamycin from the nanovehicle in vitro is much faster under NIR laser irradiation at 808 nm (Fig. 3*B*): over 90% of DOX and 15% rapamycin are released within 30 min compared with 20% and 5%, respectively, without the laser, suggesting that the nanovehicles have potential to enhance delivery by photothermal therapy under NIR laser irradiation.

Combination cancer therapy is effective due to synergistic effects that inhibit multidrug resistance (MDR). We calculate the combination index, which indicates the type and amount of interaction between two or more drugs with respect to experimental parameters (IC_{50}), for the drugs in this study (21, 22, 34, 35). The corresponding isobologram of the docetaxel-plus-afatinib combination on MCF-7 cell death after 24-h incubation at 37 °C indicates that the drug combination has a synergistic effect on MCF-7 breast cancer cells (*SI Appendix*, Fig. S5). Similar results are also shown for docetaxel-plus-rapamycin and rapamycin-plus-afatinib (*SI Appendix*, Fig. S6). We further investigate the effect on MDR by measuring and comparing the in vitro cell viability when afatinib-resistant SKBR-3/AR cells are exposed to one-, two-, and three-drug combinations delivered by the nanovehicles. The drug combinations enhance cell death compared with the single drugs, indicating that they work synergistically, as shown in Fig. 3*C*. As expected, the combination of docetaxel, rapamycin, and afatinib exhibits very strong cytotoxicity toward SKBR-3/AR cells, thus confirming that MDR has been inhibited in the cells. Additionally, photothermal therapy significantly enhances the drug combinations' effectiveness against SKBR-3/AR cells, requiring only 30 min of two drugs (docetaxel plus afatinib) to achieve nearly 80% cell death (Fig. 3*D*).

To further understand the synergistic effects, we perform a human HER2 ELISA to detect and quantify full-length HER2 protein levels from the lysates of SKBR-3 cells treated by individual drugs and drug combinations for 6 h. Afatinib significantly reduces HER2 protein expression, but again, the triple drug combination works even more effectively to decrease the expression of HER2 protein through synergy (*SI Appendix*, Fig. S7). In addition, a full-length EGFR ELISA quantifying EGFR protein expression in non–small-cell lung cancer (NSCLC) cells demonstrates that a two-drug combination of afatinib with either docetaxel or rapamycin can greatly reduce EGFR levels, which further confirms the synergy between the drugs, as shown in *SI Appendix*, Fig. S7.

Our in vitro results suggest that these drug combinations delivered by hybrid polymersome nanovehicles loaded with cNPs are promising for in vivo applications. Thus, we study in vivo tumor suppression by administering the same drug combinations in a HER2-positive breast cancer mouse model. We i.v. inject PBS, blank nanovehicles, nanovehicles containing single drugs, and nanovehicles containing drug combinations into tumor-bearing nude mice (six mice per group) once every 48 h over 4 wk for a total dosage of 5 mg/kg. Due to insolubility in water, it is not possible to inject free drug solution as a treatment at the necessary concentrations. At the end of the treatment, the tumors removed from the mice are imaged (Fig. 4*A*). The triple combination of A, D, and R at total dosages of 5 and 2.5 mg/kg suppress 94.6% and 87.5% of the tumors, respectively. The triple combination at a half-dose is still more effective than double combinations of A and either D or R at 5 mg/kg, indicating that the triple combination has the strongest synergistic effect (Fig. 4*A* and *SI Appendix*, Fig. S8). The tumor growth curves and body weight of different mouse groups during the treatment period are shown in *SI Appendix*, Fig. S9. Quantification of EGFR and VEGF protein expression in the tumors after treatment shows that PBS and blank nanovehicles do not reduce the protein expression, but nanovehicles loaded with double and triple combinations significantly reduce the protein levels (*SI Appendix*, Figs. S10 and S11). These results confirm the effectiveness of the drug combinations when administered by the nanovehicle delivery system.

To map the biodistribution of the drug-loaded nanovehicles within the mice, we conduct in vivo biofluorescence imaging of tumor-bearing mice with free Cy-7 siRNA and nanovehicle-Cy7 siRNA at 2, 8, 24, and 48 h. We find that the free-Cy7 siRNA mainly aggregates in the liver and does not accumulate in the tumor. By contrast, the nanovehicle-Cy7 siRNA does accumulate in the tumor over time, as evidenced by increasing biofluorescence in the tumor (Fig. 4*B*). In addition, we do not observe clear accumulation of the nanovehicles in the spleen. Some accumulation in the liver does occur because it is part of the clearance route from the body (36). These results suggest that the nanovehicle promotes the accumulation of drugs in the tumor, implying an improved drug delivery efficiency.

Biocompatibility and tumor suppression are evaluated by performing terminal deoxynucleotidyl transferase-mediated dUTP nick end labeling (TUNEL) apoptosis studies in tumor tissues taken from the mice. After PBS and blank nanovehicle treatment, only a few apoptotic cells are detected, showing that the nanovehicles

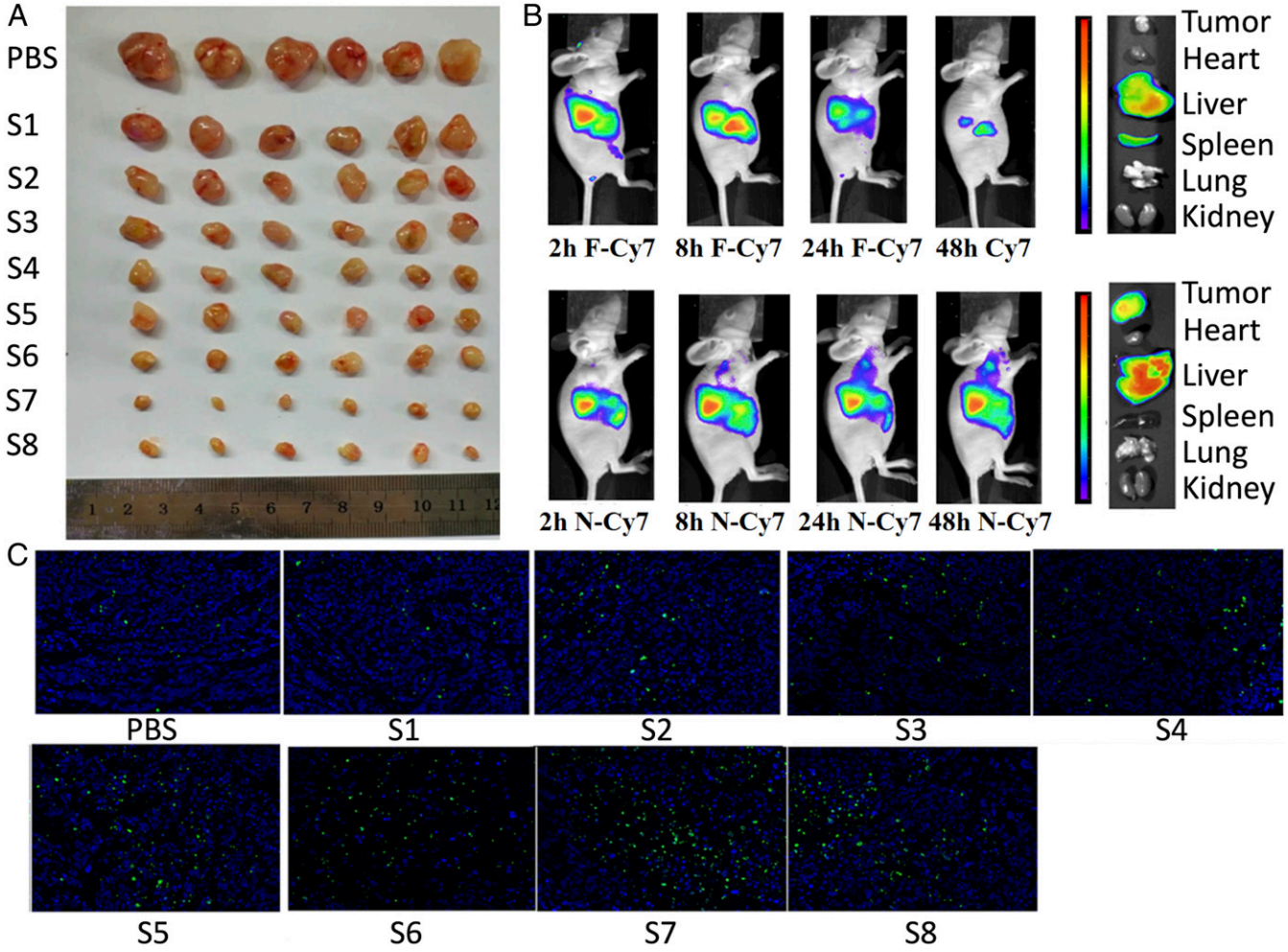

Fig. 4. The in vivo animal study through i.v. injection in mice. (*A*) The in vivo HER2-positive breast cancer tumor volume (six mice per group) after 4-wk treatment by PBS, S1 (blank nanovehicle), S2 (D-N), S3 (R-N), S4 (A-N), S5 (A+D-N), S6 (A+R-N), S7 (A+D+R-N), and S8 (A+D+R-N). The total dosage of S2 to S7 is 5 mg/kg; the total dosage of S8 for i.v. injection is 2.5 mg/kg. The drug ratio for double and triple combinations is 1–1. Nanovehicle (N): 400 μg/mL cNPs-functionalized nanosized hybrid polymersomes set up as positive control. Appearance of the tumor mass peeled off from the tumor-bearing mice at the end of study. (*B*) The in vivo biofluorescence imaging of human breast cancer tumor in mice at 2, 8, 24, and 48 h of free Cy7 (F-Cy7 siRNA) and Cy7-nanovehicle (N-Cy7 siRNA) through i.v. injection. (*C*) Terminal deoxynucleotidyl transferase-mediated dUTP nick end labeling (TUNEL) apoptosis study of tumor tissue after treatment by PBS, S1 (blank nanovehicle), S2 (D-N), S3 (R-N), S4 (A-N), S5 (D+A-N), S6 (R+A-N), S7 (D+R+A-N), and S8 (D+R+A-N). The total dosage from S2 to S7 is 5 mg/kg, and the total dosage of S8 is 2.5 mg/kg. Nanovehicle (N): The drug ratio for double and triple combinations is 1–1.

themselves are biocompatible. After treatment with drug combinations, the number of apoptotic cells increases up to about 100-fold (Fig. 4*C*). Complementary to our ELISA results, here we find that the double and triple combinations also significantly promote apoptosis as a mechanism to suppress tumor growth.

We further use immunocytochemistry to measure B-cell lymphoma 2 (Bcl-2) and Caspase 3 protein expression as a measure of apoptosis in paraffin-embedded tissue taken from the treated mice. Bcl-2 is an important antiapoptotic protein, and a significant decrease of its expression leads to marked increases in cancer cell death. Similarly, Caspase 3 is crucial mediator of apoptosis, and Caspase 3 expression increases with the number of apoptotic cells. The nanovehicle containing the three-drug combination significantly decreases Bcl-2 protein expression and increases Caspase 3 protein expression (*SI Appendix*, Fig. S12), confirming that the triple combination inhibits tumor growth through inducing cancer cell apoptosis.

Many drug delivery systems are limited by the development of significant side effects. After i.v. injection of our drug-loaded nanovehicles, H&E stains show that there is no significant toxicity or damage in the main organs of the mice, heart, liver, spleen, lung, and kidney (*SI Appendix*, Figs. S13–S17). These results suggest that the hybrid polymersome nanovehicles are effective in targeting, thus avoiding side effects (37–39). This drug combination delivered by these nanovehicles is very promising for in vivo cancer treatment.

Finally, as the range of therapeutic demands grows, the versatility of a drug delivery system becomes more important. Therefore, upon the successful delivery of the triple-drug combination, we further demonstrate that the hybrid polymersomes can load doxorubicin, anti-HER2 antibody, magnetic nanoparticles (27) (Movie S2), and double-stranded DNA (22, 40). We test the synergistic effects and MDR inhibition with SKBR-3 and SKBR-3/AR cell lines. The results indicate that the vehicle is capable of loading a wide variety of therapeutic agents that endow the vehicle with responsive properties. For example, anti-HER2 antibodies target breast cancer even more specifically than the drugs, while magnetic nanoparticles may also be useful in imaging applications. Moreover, the DNA and anti-HER2 antibodies have clear synergistic effects with the other drugs. These results are summarized in *SI Appendix*, Figs. S18 and S19.

In summary, we synthesize PSi NPs conjugated with AuNRs (cNPs) and then encapsulate the cNPs into hybrid polymersomes

composed of a biocompatible amphiphilic diblock copolymer and phospholipid shell, which is subsequently extruded to form nanovehicles. This multifunctional nanovehicle is an advanced drug delivery system with the potential to become a versatile "all-in-one" platform for therapeutics delivery. The system has high drug-loading capabilities with excellent cytocompatibility and reduced cytotoxicity to nontumor cells. Multidrug delivery by the nanovehicle both in vitro and in vivo is demonstrated using a triple combination of hydrophobic drugs (docetaxel, rapamycin, and afatinib). The drug combination very effectively inhibits MDR in HER2-positive breast cancer cells and EGFR-positive NSCLC cells through synergistic effects, especially under NIR laser irradiation. After being administered i.v. in mice, the double and triple drug combinations accumulate at the tumor due to the nanovehicles, resulting in low dosage requirements and significantly suppress cancer tumor growth and recurrence. The three-drug combination suppresses the tumor by 94% and 87% at total dosages of 5 and 2.5 mg/kg, respectively. The triple-drug combination is much more effective on tumor suppression than two-drug combinations even at half-dose. Importantly, this highly effective combination of hydrophobic drugs is only deliverable using a carrier such as these nanovehicles. The simplicity of microfluidic fabrication followed by extrusion makes the nanoplatform customizable for encapsulating and delivering various drugs and therapeutic agents as effective combination treatments for other cancer types, combined with photothermal therapy. Overall, this i.v. injectable cNPs-functionalized nanosized hybrid polymersome is a multifunctional nanovehicle for drug codelivery that holds great potential to enable new approaches to cancer therapy and other advanced biomedical applications.

Experimental Procedures

Microfluidic devices are used to produce hybrid polymersome with a shell composed of copolymer and phospholipid containing hydrophobic therapeutics afatinib, rapamycin, and docetaxel, and a core containing AuNR-conjugated PSi NPs (cNPs) coloading hydrophobic therapeutics. The loading and release of payloads, cell viability, synergistic effects, and MDR inhibition studies are investigated in cancer model cell lines. In vivo animal and bioimaging studies are performed in breast cancer mouse model by i.v. injection.

Female nude mice were fed at the condition of 25 °C and 55% of humidity and approved by the Institutional Animal Care and Use Committee of the Sixth Affiliated Hospital of Shanghai Jiao Tong University. All animal experiments were carried out in compliance with guidelines. Further detailed experimental procedures are provided in *SI Appendix*.

ACKNOWLEDGMENTS. We thank Essen BioScience for providing HeLa NucLight Red cells and two-color apoptosis/cytotoxicity demo kit and IncuCyte ZOOM for the in vitro cell apoptosis/cytotoxicity measurements. We thank Dr. Arthur McClelland at Harvard Center for Nanoscale Systems for helping with the NIR laser irradiation experiments. We are grateful to the Fundamental Research Funds for the Central Universities (FRF-BR-09-021B), 863 (2006AA03Z108) Program of China, the National Science Foundation (DMR-1708729), Harvard Material Research Science and Engineering Center (DMR-1420570), and NIH Grant R01EB023287 for financial support. H.Z., W.C., and Z.Y. acknowledge National Natural Science Foundation of China Grants 51873107, 81871472, and 51673023. H.Z. acknowledges Academy of Finland Grant 297580. H.Z. and H.A.S. acknowledge Sigrid Juselius Foundation Grants 28001830K1 and 4704580. Y.Z. and W.C. acknowledge Shanghai Municipal Education Commission–Gaofeng Clinical Medicine Grants 20152528 and 20171906, and Shanghai Jiao Tong University "Medical and Research" Program (ZH2018ZDA19 and ZH2018ZDA04).

1. Ashley CE, et al. (2011) The targeted delivery of multicomponent cargos to cancer cells by nanoporous particle-supported lipid bilayers. *Nat Mater* 10:389–397.
2. Liu D, et al. (2013) Microfluidic templated mesoporous silicon-solid lipid microcomposites for sustained drug delivery. *ACS Appl Mater Interfaces* 5:12127–12134.
3. Zhang H, et al. (2014) Fabrication of a multifunctional nano-in-micro drug delivery platform by microfluidic templated encapsulation of porous silicon in polymer matrix. *Adv Mater* 26:4497–4503.
4. Greco F, Vicent MJ (2009) Combination therapy: Opportunities and challenges for polymer-drug conjugates as anticancer nanomedicines. *Adv Drug Deliv Rev* 61:1203–1213.
5. Wang Y, et al. (2016) Lung cancer combination therapy: Co-delivery of paclitaxel and doxorubicin by nanostructured lipid carriers for synergistic effect. *Drug Deliv* 23: 1398–1403.
6. Patrick JF, et al. (2014) Continuous self-healing life cycle in vascularized structural composites. *Adv Mater* 26:4302–4308.
7. Mertz D, et al. (2012) Ultrathin, bioresponsive and drug-functionalized protein capsules. *J Mater Chem* 22:21434–21442.
8. Martino C, et al. (2012) Protein expression, aggregation, and triggered release from polymersomes as artificial cell-like structures. *Angew Chem Int Ed Engl* 51:6416–6420.
9. Liu D, et al. (2015) Microfluidic assisted one-step fabrication of porous silicon@acetalated dextran nanocomposites for precisely controlled combination chemotherapy. *Biomaterials* 39:249–259.
10. Liu D, et al. (2014) Microfluidic assembly of monodisperse multistage pH-responsive polymer/porous silicon composites for precisely controlled multi-drug delivery. *Small* 10:2029–2038.
11. Herranz-Blanco B, et al. (2014) Microfluidic assembly of multistage porous silicon-lipid vesicles for controlled drug release. *Lab Chip* 14:1083–1086.
12. Liu DF, et al. (2013) Nanostructured porous silicon-solid lipid nanocomposite: Towards enhanced cytocompatibility and stability, reduced cellular association, and prolonged drug release. *Adv Funct Mater* 23:1893–1902.
13. Wang Y, Bansal V, Zelikin AN, Caruso F (2008) Templated synthesis of single-component polymer capsules and their application in drug delivery. *Nano Lett* 8:1741–1745.
14. Yi D, et al. (2016) Synthesis of chemically asymmetric silica nanobottles and their application for cargo loading and as nanoreactors and nanomotors. *Angew Chem Int Ed Engl* 55:14733–14737.
15. Shi M, Ho K, Keating A, Shoichet MS (2009) Doxorubicin-conjugated immuno-nanoparticles for intracellular anticancer drug delivery. *Adv Funct Mater* 19:1689–1696.
16. Peyret A, Ibarboure E, Pippa N, Lecommandoux S (2017) Liposomes in polymersomes: Multicompartment system with temperature-triggered release. *Langmuir* 33:7079–7085.
17. Douglas SM, Bachelet I, Church GM (2012) A logic-gated nanorobot for targeted transport of molecular payloads. *Science* 335:831–834.
18. Schüller VJ, et al. (2011) Cellular immunostimulation by CpG-sequence-coated DNA origami structures. *ACS Nano* 5:9696–9702.
19. Vigderman L, Khanal BP, Zubarev ER (2012) Functional gold nanorods: Synthesis, self-assembly, and sensing applications. *Adv Mater* 24:4811–4841, 5014.
20. Conde J, Oliva N, Zhang Y, Artzi N (2016) Local triple-combination therapy results in tumour regression and prevents recurrence in a colon cancer model. *Nat Mater* 15: 1128–1138.
21. Kong F, et al. (2016) Gold nanorods, DNA origami, and porous silicon nanoparticle-functionalized biocompatible double emulsion for versatile targeted therapeutics and antibody combination therapy. *Adv Mater* 28:10195–10203.
22. Kong F, et al. (2015) Inhibition of multidrug resistance of cancer cells by co-delivery of DNA nanostructures and drugs using porous silicon Nanoparticles@Giant liposomes. *Adv Funct Mater* 25:3330–3340.
23. Zhang H, et al. (2018) Gold nanorods conjugated porous silicon nanoparticles encapsulated in calcium alginate nano hydrogels using microemulsion templates. *Nano Lett* 18:1448–1453.
24. Utada AS, et al. (2005) Monodisperse double emulsions generated from a microcapillary device. *Science* 308:537–541.
25. Shum HC, Kim JW, Weitz DA (2008) Microfluidic fabrication of monodisperse biocompatible and biodegradable polymersomes with controlled permeability. *J Am Chem Soc* 130:9543–9549.
26. Shum HC, et al. (2011) Dewetting-induced membrane formation by adhesion of amphiphile-laden interfaces. *J Am Chem Soc* 133:4420–4426.
27. Kong F, Zhang X, Hai M (2014) Microfluidics fabrication of monodisperse biocompatible phospholipid vesicles for encapsulation and delivery of hydrophilic drug or active compound. *Langmuir* 30:3905–3912.
28. Lee JH, Jun YW, Yeon SI, Shin JS, Cheon J (2006) Dual-mode nanoparticle probes for high-performance magnetic resonance and fluorescence imaging of neuroblastoma. *Angew Chem Int Ed Engl* 45:8160–8162.
29. Lin NU, et al. (2012) A phase II study of afatinib (BIBW 2992), an irreversible ErbB family blocker, in patients with HER2-positive metastatic breast cancer progressing after trastuzumab. *Breast Cancer Res Treat* 133:1057–1065.
30. Kah JCY, Chen J, Zubieta A, Hamad-Schifferli K (2012) Exploiting the protein corona around gold nanorods for loading and triggered release. *ACS Nano* 6:6730–6740.
31. Easton JB, Houghton PJ (2006) mTOR and cancer therapy. *Oncogene* 25:6436–6446.
32. Chang G, Ci T, Yu L, Ding J (2011) Enhancement of the fraction of the active form of an antitumor drug topotecan via an injectable hydrogel. *J Control Release* 156:21–27.
33. Minko T, Rodriguez-Rodriguez L, Pozharov V (2013) Nanotechnology approaches for personalized treatment of multidrug resistant cancers. *Adv Drug Deliv Rev* 65: 1880–1895.
34. Greco WR, Bravo G, Parsons JC (1995) The search for synergy: A critical review from a response surface perspective. *Pharmacol Rev* 47:331–385.
35. Romond EH, et al. (2005) Trastuzumab plus adjuvant chemotherapy for operable HER2-positive breast cancer. *N Engl J Med* 353:1673–1684.
36. Blanco E, Shen H, Ferrari M (2015) Principles of nanoparticle design for overcoming biological barriers to drug delivery. *Nat Biotechnol* 33:941–951.
37. Park JH, et al. (2009) Biodegradable luminescent porous silicon nanoparticles for in vivo applications. *Nat Mater* 8:331–336.
38. Hu M, et al. (2006) Gold nanostructures: Engineering their plasmonic properties for biomedical applications. *Chem Soc Rev* 35:1084–1094.
39. Chen H, Shao L, Li Q, Wang J (2013) Gold nanorods and their plasmonic properties. *Chem Soc Rev* 42:2679–2724.
40. Winfree E, Liu F, Wenzler LA, Seeman NC (1998) Design and self-assembly of two-dimensional DNA crystals. *Nature* 394:539–544.